Supplementary Information

Sulfide oxidation affects the preservation of sulfur isotope signals

Alyssa J. Findlay[a,c*], Valeria Boyko[a], André Pellerin[c], Khoren Avetisyan[a], Qingjun Guo[b†], Xi Yang[b], Alexey Kamyshny[a]

[a]Department of Geological and Environmental Sciences, Ben-Gurion University of the Negev, Beer Sheva, Israel

[b]State Key Laboratory of Resources and Environmental Information Systems, Institute of Geographic Sciences and Natural Resources Research, Chinese Academy of Sciences, Beijing, China

[c] Center for Geomicrobiology, Department of Bioscience, Aarhus University, Aarhus, Denmark

*Corresponding author: afindlay@bios.au.dk; +45 87 15 65 49

†Co-corresponding author: guoqj@igsnrr.ac.cn; +86 10 64889455

Keywords: *sulfur cycling, sulfur isotopes, paleoceanography, stratified lake, iron cycling, manganese cycling*

DR1: Study Site

Aha Reservoir (106° 37′ E, 26° 34′ N), is an artificial lake near the city of Guiyang in Guizhou Province, China with a surface area of 3.4 km^2 and a maximum depth of 24 m (Wu et al., 2001). The residence time of water in the reservoir is 0.4 – 0.5 years and the geochemistry of the lake is affected by the surrounding coal mines, which have polluted the lake with sulfate and metals (Song et al., 2011; Chen et al., 2015).

The lake is seasonally stratified during the summer and into the autumn, with stable stratification between July and September, and mixes during the winter and spring (Song et al., 2011). This yearly stratification cycle combined with the relatively short residence time means that the physical and geochemical characteristics of the water column change on seasonal time scales; however, the sulfate concentrations and bulk water column isotopic distributions at the deepest station, at which we sampled, do not appear to vary significantly over the course of the year (Song et al., 2011); although some interannual variation between this previous study ($[SO_4^{2-}]$ ~ 2.4 mM; $\delta^{34}S$ ~ -8.5 $^0/_{00}$) and ours ($[SO_4^{2-}]$ ~ 1.5 mM; $\delta^{34}S$ ~ -11 $^0/_{00}$) is apparent. Despite this variability, the water column is at quasi-steady-state during stratification, meaning that the biogeochemical processes occur faster than the physical mixing processes. This in turn means that the concentration and isotopic composition of sulfur species in the water column are affected by and show the signatures of *in situ* biogeochemical processes, such as sulfate reduction (Song et al., 2011). This is corroborated by the low variability in the chloride concentrations in the water column and sediments of the lake (Fig. S2).

Nevertheless, the seasonal cycling affects the sediment geochemistry. During the winter and spring, the water column is oxic and Fe and Mn in the sediments oxidise. Then, in the early summer, sulfate reduction and increasing organic matter decomposition reduce the upper layer of the sediments, ultimately leading to the depletion of oxygen in the water column. During this time, the sulfide produced from sulfate reduction is oxidised and dissolved Fe and Mn are subsequently released into the porewaters. Fe reacts with the sulfide produced from sulfate reduction and is retained in the sediment, whereas dissolved Mn(II) diffuses into the water column (e.g. Wu et al., 2001). By the autumn, sulfide oxidation becomes limited by the exhaustion of oxidised Fe and Mn minerals, and sulfate reduction again becomes the likely dominant processes. In the later autumn and early winter, the lake water column overturns and becomes oxic again, leading once more to accumulation of Fe

and Mn oxidised. It is this seasonal variability that refreshes the oxidant supply in the sediment and leads to the dynamic oxidation of sulfide observed in the study presented here.

DR2: Methodology

DR2.1 Sampling procedure

Water column samples were collected using an *in situ* pump. Samples were taken 10-12 August 2016 from the deepest point of the lake (24 m). The basic physical and chemical characteristics (T, conductivity, turbidity, O_2, pH) of the water column were profiled *in situ* using an Eureka Manta 2 Multiprobe Sonde. Discrete samples for further chemical analyses (SO_4^{2-}, ΣS(-II), S^0, $S_2O_3^{2-}$, SO_3^{2-}, Fe, Mn) were pumped from depth and processed immediately. Samples for SO_4^{2-}, S^0 and sulfide were preserved in zinc acetate (20 % w/v), samples for $S_2O_3^{2-}$ and SO_3^{2-} were derivatised with monobromobimane (Zopfi et al., 2004) and samples for total Fe and Mn were preserved in HCl (2 % v/v).

Sediments were collected using a gravity corer. One 35 cm core was taken and sectioned immediately into 2 cm sections for solid phase analysis. Samples for sulfur speciation were preserved in zinc acetate and frozen, samples for total metal analysis and iron speciation were frozen without preservation, and samples for porosity were kept refrigerated at 4 ^oC until analysis.

DR2.2 Analytical procedures

DR2.2.1 Water column samples

Samples for sulfide (ΣS(-II) = H_2S + HS^- + polysulfide S(-II)) preserved in zinc acetate were analysed using the spectrophotometric method of Cline (1969) with detection at 665 nm. The method detection limit is 1 µM. S^0 was extracted with chloroform and analysed using reverse phase HPLC (Agilent Technologies 1260 Infinity) on a Grace Prevail C-18 reverse phase column (250 mm length, 4.6 mm ID) with 100 % methanol as the eluent and detection at 220 and 230 nm (Kamyshny et al., 2009). Thiosulfate and sulfite were quantified by HPLC following derivatisation by monobromobimane (Zopfi et al., 2004; Newton et al., 1981). The method detection limit for both $S_2O_3^{2-}$ and SO_3^{2-} is 0.005 µM. Sulfate concentrations were measured by ion chromatography (Metrohm IC 930) with sodium carbonate/bicarbonate buffer used as the eluent.

Total iron was measured spectrophotometrically at 562 nm after addition of ascorbic acid (0.1 M) using the ferrozine method of Stookey (1970). The method detection limit is 1 µM. Total manganese was measured by the 1-(2-Pyridylazo)-2-naphthol (PAN) method according to Goto et al. (1977) after addition of ascorbic acid. The absorbance was measured at 562 nm. The method detection limit is 1 µM.

DR2.2.2 Solid phase samples

Porosity was measured by the weight loss of a known sediment volume during drying at 50 ^{o}C until a constant weight was reached (c.a. 7 days). The ratio of sediment to pore space was then calculated from the fraction of porewater in the wet sediment. Porosity decreased from 0.87 at the sediment-water interface to 0.62 at 20 cm and below.

The total organic carbon content was measured by a Rock-Eval 6 analyser (Vinci Technologies). Prior to the analysis, the wet sediment was lyophilized and 60-70 mg of dry sediment sample was combusted at 650°C for complete thermal degradation of organic matter. Organic matter was the quantified from the weight loss upon pyrolysis of the freeze-dried sediment (MDL was 0.005% TOC with a precision of 1%).

Zero-valent sulfur was extracted with pure methanol (1:30 w/v) overnight on a rotary shaker. Following extraction, the sediment was separated from the extract by centrifugation and S^0 was quantified as S_8 using reverse-phase HPLC on a C-18 column with UV/Vis detection at 265 nm and 100 % methanol as the eluent.

Acid Volatile Sulfide (AVS, consisting of H_2S, HS^-, FeS) and Chromium Reducible Sulfur (CRS, consisting mainly of FeS_2) were measured in the sediment after S^0 extraction by distillation following Fossing and Jørgensen (1989). AVS was released upon acidification of the sample with HCl (5 M) and boiling for 3 hours. CRS was released after the addition of acidic Cr(II) solution and boiling for 2 hours. The evolved sulfide was trapped as ZnS and sulfide concentrations were determined spectrophotometrically as described for the water column samples.

Total solid phase Fe and Mn were measured after 24 hours digestion in boiling HCl (6 N) following the method of Aller and Mackin (1986). Operationally defined reactive iron speciation was determined after Poulton and Canfield (2005). The reactive Fe pool was divided into the following fractions based upon extraction with different reagents: (1) Fe(II) extracted by acetate (Fe carbonates and a portion of Fe bound in the AVS pool), (2) easily reducible Fe hydroxides extracted by hydroxylamine (e.g. ferrihydrite), (3) reducible Fe oxides extracted by dithionite (e.g. hematite, goethite) and (4) poorly crystalline Fe oxides extracted by ammonium oxalate (e.g. magnetite). Iron concentrations in the digestion and all extractions were measured spectrophotometrically via the ferrozine method and total manganese from the acid digestion was measured by the PAN method as described above for water samples.

DR2.2.3 Sulfur isotopic composition

Samples for both porewater and water column sulfate were prepared for isotopic analysis by STRIP reagent reduction (Arnold et al., 2014), during which the evolved hydrogen sulfide was trapped as Ag_2S. Water column AVS was precipitated from 1 - 10 L samples (depending on sulfide concentration) as ZnS and filtered. The ZnS on the filters was then distilled with 5 M HCl and the evolved H_2S was trapped as Ag_2S. ZnS trapped after distillation of sedimentary AVS and CRS was converted to Ag_2S upon addition of $AgNO_3$ (1 M). Sedimentary S^0 was prepared for isotopic analysis by evaporating >90 % of the methanol extract on a rotary evaporator. Sulfur was extracted from the remaining methanol-water mixture with dichloromethane, which was then evaporated under nitrogen flow, and elemental sulfur was reduced by Cr(II) after the method of Gröger et al. (2009). The evolved hydrogen sulfide was trapped as Ag_2S.

All Ag_2S precipitates were aged for one week, washed thrice with 18.2 MΩ water (MilliQ), left overnight in diluted NH_4OH (1 M), then were washed once more with 18.2 MΩ water. Cleaned samples were dried overnight at 60 ^oC. Silver sulfide was converted to SF_6 by reaction with excess F_2 at 300 ^oC for at least 10 hours in Monel reaction chambers. The SF_6 was then purified cryogenically and by preparative gas chromatography (Ono et al., 2006). Following purification, stable sulfur isotopic measurements (^{32}S, ^{33}S, ^{34}S) were conducted on a Finnigan MAT 253 dual inlet mass spectrometer.

Isotopic composition is presented in permille using standard δ notation relative to VCDT (Eq. 1)

$$\delta^{3x}S = ({}^{3x}R_{sample}/{}^{3x}R_{VCDT} - 1) \times 1000 \qquad (1)$$

in which ${}^{3x}R = {}^{3x}S/{}^{32}S$ (x=3 or 4).

The minor isotope composition is presented using $\Delta^{33}S$ notation (Eq. 2), which describes the deviation of $\delta^{33}S$ from a reference fractionation line (Farquhar and Wing, 2003).

$$\Delta^{33}S = \delta^{33}S - 1000 \times ((1 + \delta^{34}S/1000)^{0.515} - 1) \qquad (2)$$

DR3: Model of multiple sulfur isotopes

DR3.1 Description and equations

Despite the observation that sulfide oxidation, rather than sulfate reduction is the net processes in the surface sediments of Aha Reservoir, this is not sustainable over long time periods, as eventually all sulfide would be re-oxidised. This situation is therefore likely seasonal and we suggest that the system is not at steady-state over seasonal timescales. However, dissolved species in the porewater can reach steady-state conditions over relatively short timescales without the solid phase being significantly affected. The typical equilibration

time for diffusive fluxes on the centimetre scale is 1-2 days (Iverson and Jørgensen, 1993). Given that the bottom water conditions in Aha Reservoir only vary seasonally, this means that the porewater species will be at steady state during these timescales. Therefore, the application of a box model, derived after Pellerin et al. (2014) to describe porewater sulfur transformations is justified.

The model considers three processes: (1) sulfide (AVS) oxidation (associated with low fractionation), (2) disproportionation (associated with high fractionation) and (3) sulfate reduction (associated with high fractionation) (Fig. S5). We note that SO_4^{2-} in this system is also lost to diffusion, which we assumed is a non-fractionating process (Wortmann and Chernyavsky, 2011). These processes are described by the following equations. The isotopic fractionation between a product and the reacting pool is described by Eq. 3

$$^{3i}R_{product} = {}^{3i}\alpha_{path}\ {}^{3i}R_{Reactant} \qquad (3)$$

in which ^{3i}R represents the isotopic ratio, where i = 3 or 4 ($^{34}S/^{32}S$ or $^{33}S/^{32}S$) and $^{3i}\alpha_{path}$ represents the fractionation factor associated with the specific process (e.g. oxidation or reduction). The relationship between $^{34}\alpha_{path}$ and $^{33}\alpha_{path}$ is $^{33}\alpha_{path} = {}^{34}\alpha_{path}{}^{\lambda}$, where λ is constrained by previously established ranges for each process.

Sulfate reduction can be represented as $^{3i}\alpha_{red} = \frac{^{3i}R_{SO4,\varphi red}}{^{3i}R_{SO4}}$ ($^{3i}R_{SO4}\varphi_{red}$ is the isotopic ratio of the SO_4^{2-} being reduced to AVS, thereby leaving the sulfate pool and $^{3i}R_{SO4}$ is the porewater sulfate). For the case of AVS oxidation, $^{3i}\alpha_{AVS-Si} = \frac{^{3i}R_{AVS,\varphi ox}}{^{3i}R_{AVS}}$ ($^{3i}R_{AVS}\varphi_{ox}$ is the AVS being oxidised to S_i and $^{3i}R_{AVS}$ is the bulk AVS).

To differentiate the effects of both SO_4^{2-} formation through disproportionation of S_i and direct AVS oxidation to SO_4^{2-}, φ_{ox} is further broken down into two fluxes, φ_{ox_disp} and φ_{ox_dir} with a relationship which follows the mass balance in Eq. 4

$$1 = f_{ox\_disp} + f_{ox\_dir} \qquad (4)$$

where $f_{ox\_disp} = \frac{\varphi_{ox\_disp}}{\varphi_{ox}}$ and $f_{ox\_dir} = \frac{\varphi_{ox\_dir}}{\varphi_{ox}}$. We do not assign a separate fractionation to f_{ox_dir} (i.e. $^{3i}\alpha_{ox\_dir} = {}^{3i}\alpha_{AVS-Si}$); thus, the net fractionation due to sulfide oxidation can be described as follows (Eq. 5)

$$^{3i}\alpha_{ox} = {}^{3i}\alpha_{ox\_disp} \cdot f_{ox\_disp} + {}^{3i}\alpha_{AVS-Si} \cdot \left(1 - f_{ox\_disp}\right) \qquad (5)$$

where ${}^{3i}\propto_{ox\_disp}=\frac{{}^{3i}R_{AVS,\phi ox\_disp}}{{}^{3i}R_{AVS}}$ is the fractionation produced from the disproportionation pathway (the isotopic ratio of the material leaving the AVS pool and the isotopic ratio of the AVS pool).

Disproportionation includes the oxidation of AVS to the intermediate species S_i followed by disproportionation. This results in a partial oxidation of S_i to SO_4^{2-} and a partial reduction back to AVS, represented by Eq. 6

$$ {}^{3i}\propto_{disp}=\frac{{}^{3i}\propto_{AVS-Si}}{f_{S_i-AVS}\left(\frac{{}^{3i}\propto_{S_i-AVS}}{{}^{3i}\propto_{S_i-SO_4}}-1\right)+1} \qquad (6)$$

in which ${}^{3i}\propto_{S_i\_AVS}=\frac{{}^{3i}R_{Si\ disp\ red}}{{}^{3i}R_{Si}}$ represents the fractionation between AVS produced from S_i reduction and the S_i pool, ${}^{3i}\propto_{S_i\_SO_4}=\frac{{}^{3i}R_{Si\ disp\ ox}}{{}^{3i}R_{Si}}$ represents the fractionation between SO_4^{2-} produced from S_i oxidation and the bulk S_i pool and f_{S_i-AVS} represents the stoichiometry of the disproportionation reaction taking place (0.75 for S^0 disproportionation, 0.25 for SO_3^{2-} disproportionation, 0.5 for $S_2O_3^{2-}$ disproportionation).

The fractionations associated with each process result in an observed fractionation between end-member pools (i.e. AVS and SO_4^{2-}), which is defined by Eq. 7

$$ {}^{3i}\propto_{\underline{SO4-AVS}}=\frac{{}^{3i}R_{SO4}}{{}^{3i}R_{AVS}} \qquad (7)$$

The prevailing processes of the sulfur cycle can then be described by Eq. 8

$$ {}^{3i}\propto_{\underline{SO4-AVS}}=\frac{{}^{3i}\propto_{ox}}{f_{red}({}^{3i}\propto_{red}-1)+1} \qquad (8)$$

in which f_{red} corresponds to the fraction of SO_4^{2-} sourced from AVS oxidation, which is then re-reduced to AVS.

The mass balance is $f_{red}=\frac{\phi_{red}}{\phi_{ox}}$. ${}^{3i}\propto_{ox}$ is generally >1 for chemical sulfide oxidation and disproportionation and ${}^{3i}\propto_{red}$ is < 1 for SO_4^{2-} reduction.

DR3.2 Model scenarios

Three different combinations of the processes described above were tested to try to recreate the observed $\delta^{34}S_{sulfate\text{-}AVS}$ and $\Delta^{33}S_{sulfate\text{-}AVS}$ values. Two combinations were not able to recreate the measured fractionations: (1) Sulfide (AVS) oxidation without sulfate reduction and (2) disproportionation of an intermediate sulfur species following sulfide oxidation, whereas Scenario (3) was able to reproduce the observed data. The details of these scenarios are described below:

Scenario 1: Sulfide (AVS) oxidation without sulfate reduction. Here, we varied the fractionation factor associated with sulfide oxidation fractionation between -5 and 5 $^{0}/_{00}$ (Fry et al., 1986; Fry et al., 1988) utilizing λ of 0.515 (Zerkle et al., 2009). This varies the resulting net fractionation only marginally and does not reproduce the data from Aha Reservoir. Sulfide oxidation alone is therefore unlikely to be the dominant fractionating process in Aha Reservoir.

Scenario 2: Disproportionation of an intermediate sulfur species following sulfide oxidation. To establish the range of fractionations which can be produced by a combination of sulfide oxidation and disproportionation in Aha Reservoir, we again varied sulfide oxidation from -5 to +5 $^{0}/_{00}$ and considered elemental sulfur disproportionation based on published fractionation values ($\varepsilon_{Si\text{-}SO4}$ = 18.53, $\lambda_{Si\text{-}SO4}$ = 0.5195 $\varepsilon_{Si\text{-}H2S}$ = -6.18, $\lambda_{Si\text{-}H2S}$ = 0.5165) observed with pure cultures of elemental sulfur disproportionating bacteria (Johnston et al., 2005). This can be repeated for disproportionation of $S_2O_3^{2-}$ or SO_3^{2-} without changing the conclusions, as the resulting fractionations are similar. The combination of sulfide oxidation and disproportionation approach the measured values, however, it is only with the addition of sulfate reduction that the model solution encloses the observed fractionations.

Scenario 3: Here, we varied sulfide oxidation from -5 to +5 $^{0}/_{00}$, considered elemental sulfur disproportionation based on published fractionation values ($\varepsilon_{Si\text{-}SO4}$ = 18.53, $\lambda_{Si\text{-}SO4}$ = 0.5195 $\varepsilon_{Si\text{-}H2S}$ = -6.18, $\lambda_{Si\text{-}H2S}$ = 0.5165) observed with pure cultures of elemental sulfur disproportionating bacteria (Johnston et al., 2005), and added sulfate reduction as a fractionating process. Only large fractionations ($\varepsilon_{SO4\text{-}AVS}$) can reproduce the isotopic signatures observed in the upper sediment; sulfate reduction at lower ε (e.g. at the observed fractionation in the water column of Aha Reservoir, 30 $^{0}/_{00}$) does not reproduce the data. Disproportionation was not necessary to reproduce the observed values.

230 **Figure DR1:** (A) Physical structure of the water column, (B) Concentrations of intermediate
231 sulfur species

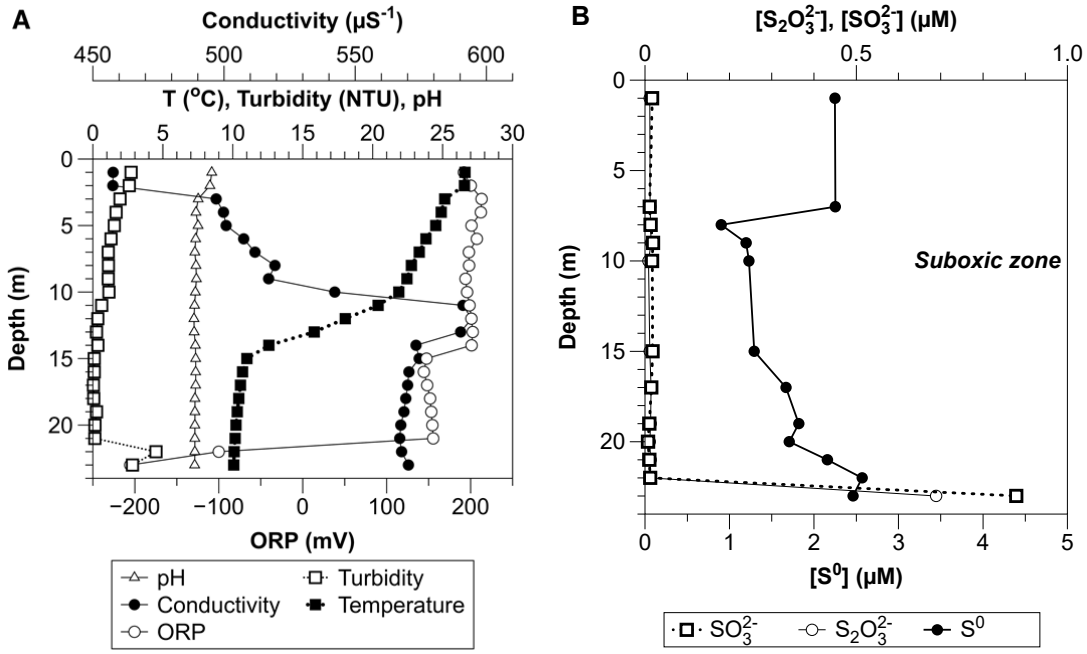

Figure DR2: (A) Distribution of total Fe, Fe_{HR} and total Mn in the sediment and (B) Reactive Fe (Fe_{HR}) speciation in the sediment.

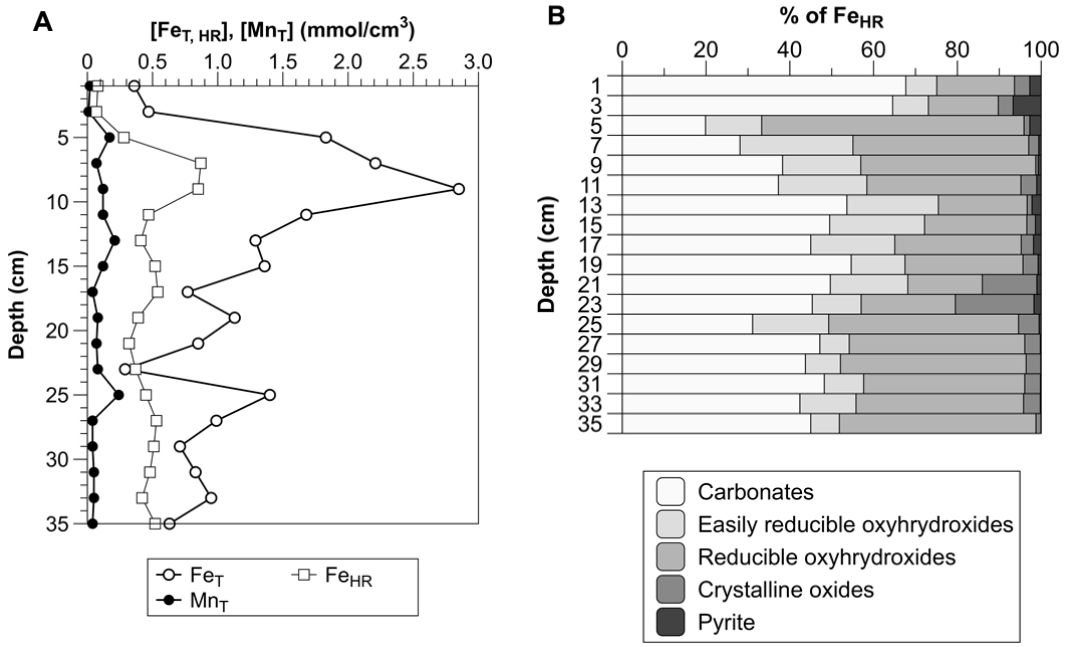

234 **Figure DR3:** Chloride concentrations in (A) the water column and (B) the sediment.

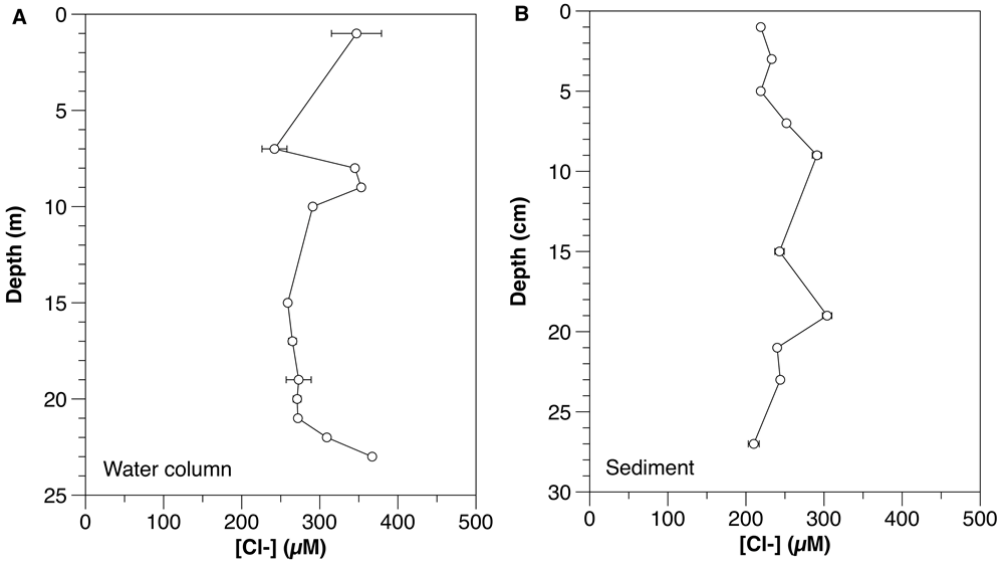

Figure DR4: $\Delta^{33}S$ of sedimentary sulfur species. The error bars represent 1σ (0.02 $^{0}/_{00}$).

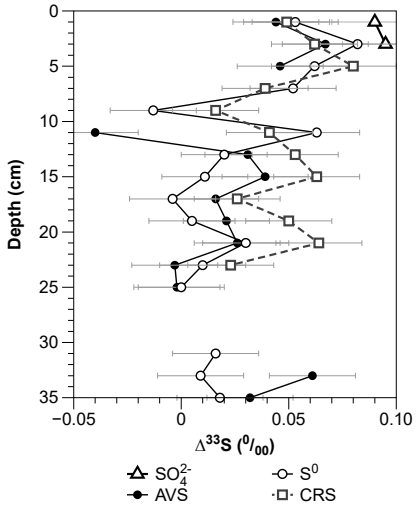

Figure DR5: Conceptual diagramme of the sulfur pools and transformations considered in the model.

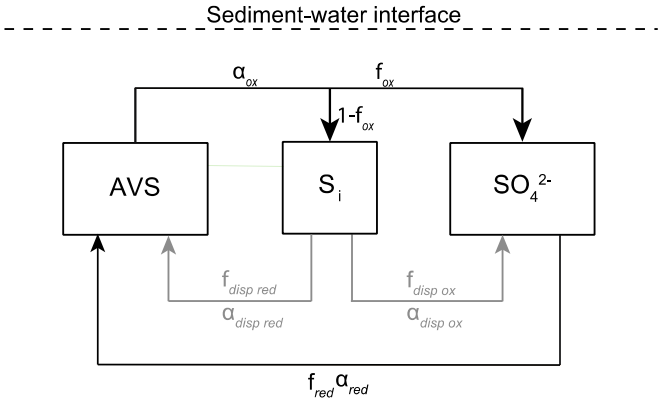

References

Aller, R.C., Mackin, J.E. and Cox, R.T.,, 1986 Diagenesis of Fe and S in Amazon inner shelf muds: apparent dominance of Fe reduction and implications for the genesis of ironstones. *Cont. Shelf Res.* v. 6, p. 263–289.

Arnold, G.L., Brunner, B., Müller, I.A. and Røy, H., 2014, Modern applications for a total sulfur reduction distillation method - what's old is new again. *Geochem. T.* v. 15:4.

Cline, J., 1969, Spectrophotometric determination of hydrogen sulfide in natural waters. *Limnol. Oceanogr.* v. 14, p. 454–458.

Farquhar, J. and Wing, B.A., 2003, Multiple sulfur isotopes and the evolution of the atmosphere. *Earth Planet. Sc. Lett.* v. 213, p. 1–13.

Fossing, H. and Jorgensen, B.B., 1989, Chromium reduction method of bacterial sulfate reduction in sediments: Measurement reduction of a single-step chromium method Evaluation. *Biogeochemistry* v. 8, p. 205–222.

Fry, B., Cox, J., Gest, H. and Hayes, J.M., 1986, Discrimination Between S-34 and S-32 During Bacterial Metabolism of Inorganic Sulfur-Compounds. *J. Bacteriol.* v. 165, p. 328–330.

Fry, B., Gest, H. and Hayes, J.M., 1988, $^{34}S/^{32}S$, fractionation in sulfur cycles catalyzed by anaerobic bacteria. *Appl. Environ. Microbiol.* v. 54, p. 250–256.

Goto, K., Taguchi, S., Fukue, Y. and Ohta, K., 1977, Spectrophotometric determination of manganese with 1-(2-pyridylazo)-2-naphthol and a non-ionic surfactant. *Talanta* v. 24, p. 752–753.

Gröger, J., Franke, J., Hamer, K. and Schulz, H.D., 2009, Quantitative recovery of elemental sulfur and improved selectivity in a chromium-reducible sulfur distillation. *Geostand. Geoanal. Res.* v. 33, p. 17–27.

Iversen, N. and Jørgensen, B.B., 1993, Diffusion coefficients of sulfate and methane in marine sediments: Influence of porosity. *Geochim. Cosmochim. Ac*. v. 57, p. 571-578. doi: 10.1016/0016-7037(93)90368-7.

Johnston, D.T., Wing, B.A., Farquhar, J., Kaufman, A.J., Strauss, H., Lyons, T.W., Kah, L.C. and Canfield, D.E., 2005, Active Microbial Sulfur Disproportionation in the Mesoproterozoic. *Science* v. 310, p. 1477–1479.

Kamyshny Jr., A., Borkenstein, C.G. and Ferdelman, T.G., 2009 Protocol for quantitative detection of elemental sulfur and polysulfide zero-valent sulfur distribution in natural aquatic samples. *Geostand. Geoanalytical Res.* v. 33, p. 415–435.

Newton, G.L., Dorian, R. and Fahey, R.C., 1981, Analysis of biological thiols: Derivatization with monobromobimane and separation by reverse-phase high-performance liquid chromatography. *Anal. Biochem.* v. 114, p. 383–387.

Ono, S., Wing, B., Rumble, D., Farquhar, J., 2006, High precision analysis of all four stable isotopes of sulfur (^{32}S, ^{33}S, ^{34}S and ^{36}S) at nanomole levels using a laser fluorination isotope-ratio-monitoring gas chromatography-mass spectrometry. *Chem. Geol.* v. 225, p. 30–39.

Poulton, S.W. and Canfield, D.E., 2005, Development of a sequential extraction procedure for iron : implications for iron partitioning in continentally derived particulates. *Chem. Geol.* v. 214, p. 209–221.

Song, L., Liu, C., Wang, Z., Teng, Y., Wang, J., Liang, L. and Bai, L., 2011, Seasonal variations in sulfur isotopic composition of dissolved SO_4^{2-} in the Aha Lake, Guiyang and their implications. *Chin. J. Geochem.* v. 30, p. 444–452.

Stookey, L.L., 1970, Ferrozine-A New Spectrophotometric Reagent for Iron. *Anal Chem* v. 42, p. 779–781.

Wortmann, U.G. and Chernyavsky, B., 2011, The significance of isotope specific diffusion coefficients for reaction-transport models of sulfate reduction in marine sediments. *Geochim. Cosmochim. Ac.* v. 75, p. 3046-3056.

Wu, F.C., Wan, G.J., Huang, R.G., Pu, Y. and Cai, Y.R., 2001, Geochemical processes of iron and manganese in a seasonally stratified lake affected by coal-mining drainage in China. *Limnology* v. 2, p. 55–62.

Zerkle, A.L., Farquhar, J., Johnston, D.T., Cox, R.P. and Canfield, D.E., 2009, Fractionation of multiple sulfur isotopes during phototrophic oxidation of sulfide and elemental sulfur by a green sulfur bacterium. *Geochim. Cosmochim. Acta* v. 73, p. 291–306.

Zopfi, J., Ferdelman, T.G. and Fossing, H., 2004, Distribution and fate of sulfur intermediates - sulfite, tetrathionate, thiosulfate and elemental sulfur - in marine sediments. *Spec. Pap. Geol. Soc. Am.* v. 379, p. 17–34.